JOC The Journal of Organic Chemistry

Article

pubs.acs.org/joc

Phototautomerization in Pyrrolylphenylpyridine Terphenyl Systems

Nikola Basarić,*[,†] Suma S. Thomas,[‡] Vesna Blažek Bregović,[†] Nikola Cindro,[†] and Cornelia Bohne*[,‡]

[†]Department of Organic Chemistry and Biochemistry, Ruđer Bošković Institute, Bijenička cesta 54, 10 000 Zagreb, Croatia

[‡]Department of Chemistry, University of Victoria, Box 3065 STN CSC, Victoria, BC V8W 3 V6, Canada

Supporting Information

ABSTRACT: [4-(2-Pyrrolyl)phenyl]pyridines **2**–**4** were synthesized and their photophysical properties and reactivity in phototautomerization reactions investigated by fluorescence spectroscopy and laser flash photolysis (LFP). The pK_a for the protonation of the pyridine nitrogen in **2**–**4** was determined by UV–vis and fluorescence titration (pK_a = 5.5 for **4**). On excitation in polar protic solvents, **2**–**4** populate charge-transfer states leading to an enhanced basicity of the pyridine (pK_a* ≈ 12) and enhanced acidity of pyrrole (pK_a* ≈ 8–9) enabling excited-state proton transfer (ESPT). ESPT gives rise to phototautomers and significantly quenches the fluorescence of **2**–**4**. Phototautomers **2-T** and **4-T** were detected by LFP with strong transient absorption maxima at 390 nm. Phototautomers **2-T** and **4-T** decayed by competing uni- and bimolecular reactions. However, at pH 11 the decay of **4-T** followed exponential kinetics with a rate constant of 4.2 × 10^6 s^{-1}. The pyridinium salt **4H**$^+$ forms a stable complex with cucurbit[7]uril (CB[7]) with 1:1 stoichiometry (β_{11} = (1.0 ± 0.2) × 10^5 M^{-1}, [Na^+] = 39 mM). Complexation to CB[7] increased the pK_a for **4H**$^+$ (pK_a = 6.9) and changed its photochemical reactivity. Homolytic cleavage of the pyrrole NH leads to the formation of an N-radical because of the decreased acidity of the pyrrole in the inclusion complex.

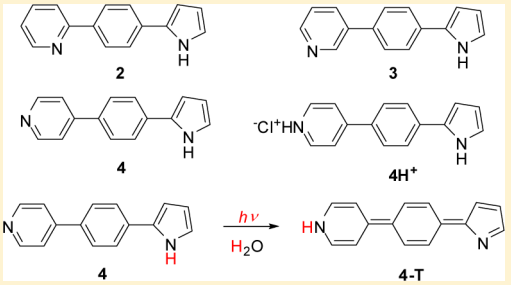

INTRODUCTION

Proton transfer is a fundamental reaction in chemistry and biology[1] that has received much attention due to its fundamental aspects as well as numerous applications.[2] Upon electronic excitation, some organic functional groups exhibit enhanced acidity or basicity.[3,4] If these sites are in close proximity, excitation can lead to excited-state intramolecular proton transfer (ESIPT).[5−8] However, if the basic and acidic sites are not at a short distance, proton transfer can be feasible either via double-proton transfer or via a relay mechanism over bridges of protic molecules.[9] The latter process is particularly interesting in biological systems and involves chains of polar amino acids and H_2O molecules[10−12] or coupled electron transfer and proton transfer.[13,14] Long-range proton transfer also takes place in respiratory complexes,[15] whereas absorption of light in bacteriorhodopsin enables the function of a proton pump that moves protons through a membrane against a gradient.[16,17] The mechanism of ESPT that involves solvent-relay shuffling of a proton has been documented for 7-azaindoles[18] and 7-hydroxyquinoline[19−23] and has been used for the probing of structural dynamics in proteins.[24] Furthermore, proton transfer taking place via relay of H_2O molecules has been used to study dynamics of membranes and micelles.[25−27]

ESIPT in the pyrrolylpyridine systems has been well documented.[28] In these examples, the pyrrole or indole NH is the acidic site, whereas the pyridine nitrogen is the basic site.[29−33] For example, photoexcitation of pyrrolylpyridine **1** in nonpolar solvents leads to ESIPT and to the population of phototautomer **1-T** (eq 1), which was detected by fluorescence spectroscopy.[31] In the corresponding *m*- and *p*-pyridine

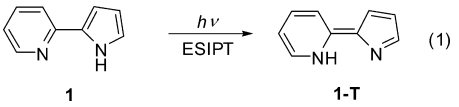

(1)

derivatives wherein the acidic and basic sites are distant, solvent-assisted double-proton transfer occurs, giving rise to phototautomers or H-bonding complexes with the solvent, leading to a de-excitation via an internal conversion channel.[34−36]

Herein we report on the investigation of solvent-assisted phototautomerization (formal proton transfer) in a series of pyrrolylphenylpyridine terphenyl derivatives **2**–**4**. The photophysical properties of molecules **2**–**4** were investigated by fluorescence spectroscopy, whereas formation of the phototautomers was probed by laser flash photolysis (LFP). Furthermore, the complexation of **4H**$^+$ with cucurbit[7]uril (CB[7]) was investigated because inclusion complexes with CB[*n*]s were shown to alter photochemical reactivity[37] and these complexes have been the focus of intensive research,[38] particularly owing to their potential applicability as drug delivery vehicles[39−41] or photoswitches.[42,43] Herein we demonstrate that complexation of **4H**$^+$ with CB[7] changes its photochemical reactivity and prevents phototautomerization.

RESULTS

Synthesis. Pyrrole derivatives **2**–**4** were prepared from the corresponding (4-bromophenyl)pyridines (Schemes 1–3).

Received: February 5, 2015
Published: March 30, 2015

DOI: 10.1021/acs.joc.5b00275
J. Org. Chem. 2015, 80, 4430−4442

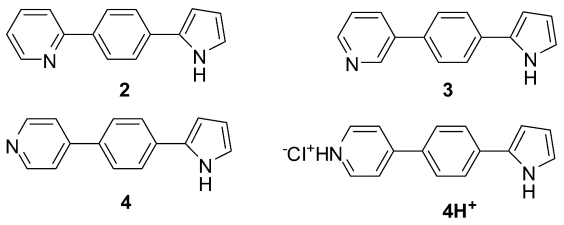

Scheme 1

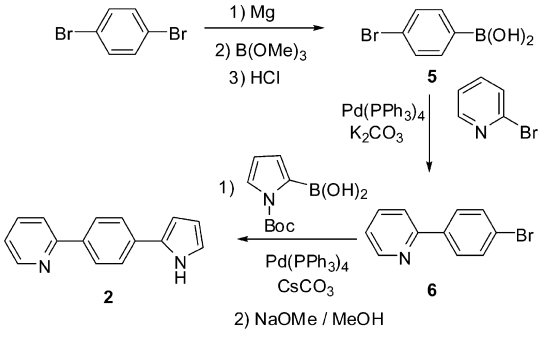

For the *ortho* derivative, (4-bromophenyl)boronic acid (**5**) was prepared first, that in the Suzuki coupling with 2-bromopyridine afforded 2-(4-bromophenyl)pyridine (**6**)[44,45] in a yield of 29%. The subsequent Suzuki reaction with the pyrrole boronic acid,[46] according to the optimized conditions for the arylation of pyrrole[47] and the Boc-deprotection in basic conditions (Scheme 1), gave the target compound **2**.[48]

Synthesis of *meta* derivative **3** started from the commercially available 3-pyridineboronic acid that was arylated in a Suzuki coupling to afford bromide **7**[49,50] and subsequently reacted in another Suzuki coupling with pyrroleboronic acid to give **3-Boc** derivative. Boc deprotection under basic conditions gave the target compound in an overall yield of ∼20% (Scheme 2).

Scheme 2

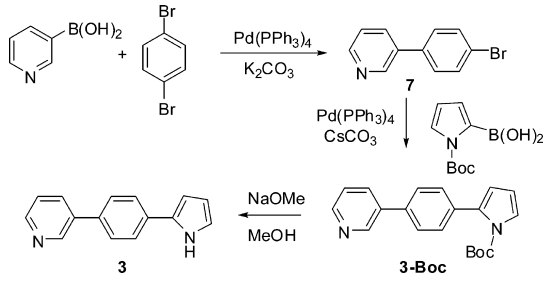

The synthetic strategy for *para* derivative **4** was different than for **2** and **3** since bromide **8** was not prepared in a metal-catalyzed cross-coupling. Instead, according to a modification of the published procedure,[51] pyridine was activated by transforming it to a triflate salt, which enabled nucleophilic addition of *p*-bromophenyllithium generated in situ. The reaction gave the 1,2- (minor) and 1,4-adducts (major) which were isolated as a mixture and without characterization treated with a base to afford **8**[48] as the major product, isolated in the overall yield of 25%. Subsequent arylation with pyrroleboronic acid, as for the *ortho* and *meta* derivative, and Boc deprotection gave the target compound (Scheme 3).

Fluorescence Measurements. Absorption spectra of **2**–**4** taken in CH_3CN (Figure 1, top) exhibit an absorption band

Scheme 3

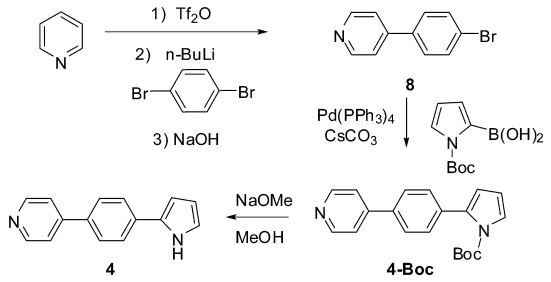

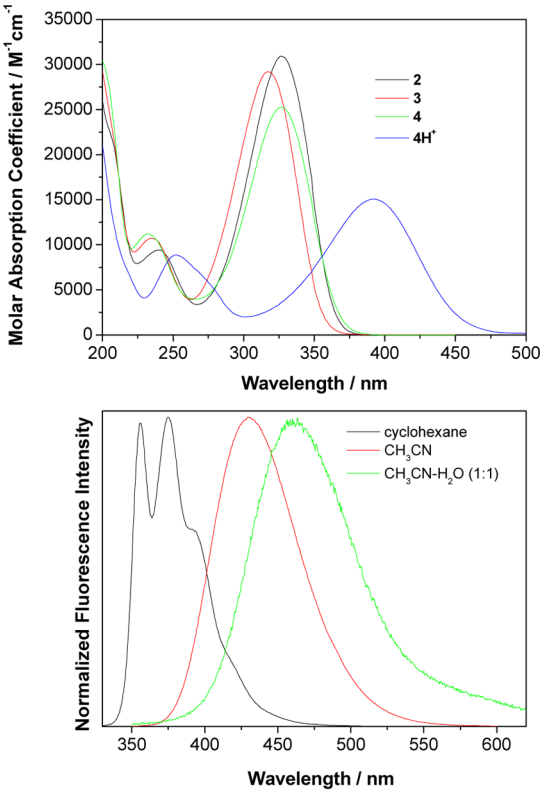

Figure 1. Absorption spectra of **2**–**4** and **4H**$^+$ in CH_3CN (top) and normalized fluorescence spectra of **4** in different solvents (bottom).

with a maximum at around 327 nm corresponding to the HOMO–LUMO transition and population of S_1. The geometries of the two conformers of **4** and orbitals involved in the electronic transition are presented in the Supporting Information (Figure S1 and S2 and Tables S1, S3, and S4). The excitation has a significant charge-transfer (CT) character, leading to an electron-density enhancement on the pyridine and a decrease on the pyrrole.

Fluorescence spectra of **2**–**4** were measured in cyclohexane, CH_3CN, and CH_3CN–H_2O (1:1, Figure 1, bottom, and Figures S5–S12 in the Supporting Information). In cyclohexane, the fluorescence spectra of **2**–**4** are structured with a vibronic progression of 1400 cm^{-1}. The increase in solvent polarity shifts the maximum of the emission to longer wavelengths (Figure 1, bottom, and Figures S7, S9, and S11 in the Supporting Information) and leads to a disruption of the vibronic structure. These findings suggest an increase of the dipole moment for the excited state, in agreement with the calculation for **4** (see Table S3, Supporting Information).

DOI: 10.1021/acs.joc.5b00275
J. Org. Chem. 2015, 80, 4430–4442

Table 1. Photophysical Properties of 2−4 and 4H$^+$

	Φ^a (cyclo)	τ^b (cyclo) (ns)	Φ^a (CH_3CN)	τ^b (CH_3CN) (ns)	Φ^a (CH_3CN–H_2O)	τ^b (CH_3CN–H_2O) (ns)
2	0.90 ± 0.03	(60−120) × 10^{-3} 1.25 ± 0.01	0.95 ± 0.05	2.14 ± 0.01	0.046 ± 0.003	(90−120) × 10^{-3} 0.40 ± 0.05
3	0.90 ± 0.02	(70−100) × 10^{-3} 1.25 ± 0.01	0.83 ± 0.03	2.28 ± 0.01	(2.7 ± 0.2) × 10^{-3}	<30 × 10^{-3}
4	0.95 ± 0.02	(60−100) × 10^{-3} 1.41 ± 0.01	0.91 ± 0.03	2.29 ± 0.01	0.049 ± 0.003	(90−150) × 10^{-3} 0.3 ± 0.1
4H$^+$			0.012 ± 0.002[c]	0.11 ± 0.01 0.68 ± 0.02		

[a]Fluorescence quantum yields measured by use of quinine sulfate in 0.05 M H_2SO_4 as a reference (Φ_f = 0.53).[52] Errors correspond to averaged data measured at three different wavelengths. [b]Measured by SPC. Errors correspond to those obtained by global fitting of three decays at different emission wavelengths. The pre-exponential factors for the fastest lifetime of the nonexponential decays were: 0.03−0.05 in cyclohexane, 0.6−0.95 in CH_3CN–H_2O with a significant dependence on the emission wavelengths, and 0.4−0.5 for **4H**$^+$ in CH_3CN. [c]Estimated fluorescence quantum yield measured for the emission band at 570 nm by use of acridine yellow in CH_3OH as a reference (Φ_f = 0.57).[53] Errors correspond to averaged data measured at three different wavelengths.

Scheme 4. Phototautomerization of 4 and Formation of Its Radical in Aqueous Solution Depending on pH

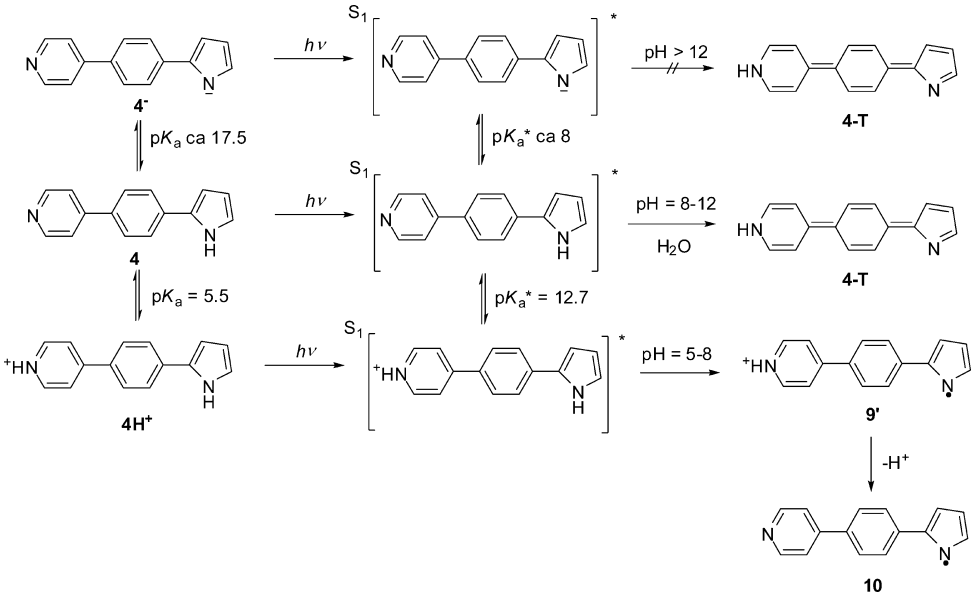

Quantum yields of fluorescence for **2−4** were measured by use of quinine sulfate/0.05 M H_2SO_4 as a reference (see equation S1 in the Supporting Information), whereas lifetimes were measured by time-correlated single-photon counting (SPC). Similar quantum yields were measured for **2−4** in cyclohexane and CH_3CN (Table 1). The decays from S_1 for **2−4** were faster in cyclohexane than in CH_3CN, and in cyclohexane the kinetics were fit to a sum of two exponentials, while they were fit to a monoexponential function in CH_3CN (Table 1). Although straightforward assignment of decay components in cyclohexane is not possible at this point, the observation could be interpreted as due to locally excited (LE) and charge-transfer (CT) states, or aggregation of molecules in that solvent. However, the fine vibronic structure observed in the steady-state spectra in cyclohexane does not suggest aggregation. Nevertheless, in CH_3CN only one S_1 state is populated with a significant CT character wherein the pyrrole moiety becomes relatively positively charged (and, therefore, more acidic than in S_0) and the pyridine relatively negatively charged (more basic than in S_0).

Protonation of the pyridine nitrogen in **4H**$^+$ significantly shifts the position of the absorption maximum bathochromically to 393 nm (Figure 1, top) owing to a larger stabilization of S_1 than S_0 by protonation of **4**. However, dilution of the solution (from 5 × 10^{-5} to 5 × 10^{-6} M) changes the appearance of the spectrum with the shift of the maximum to 327 nm (Figure S13, Supporting Information). Although these spectral changes could be related to deaggregation of the molecules by dilution, the spectral changes are consistent with the deprotonation of **4H**$^+$ because the changes parallel those observed in the pH titration. Therefore, **4H**$^+$ in CH_3CN behaves as a weak acid suggesting that both **4** and **4H**$^+$ are present in solution.

Fluorescence spectra of **4H**$^+$ in CH_3CN are also strongly dependent on concentration (Figure S14, Supporting Information) with two emission maxima at 430 and 570 nm, corresponding to **4** and **4H**$^+$, respectively. Moreover, the fluorescence decay of **4H**$^+$ in CH_3CN is biexponential due the presence of **4** and **4H**$^+$. The fluorescence quantum yield of **4H**$^+$ in CH_3CN (c = 5 × 10^{-6} M) measured for the emission between 430 and 750 nm was estimated by exciting the sample at ca. 410 nm where only **4H**$^+$ absorbs, giving a value about 75 times lower than for **4**. Increase of temperature also led to the deprotonation of **4H**$^+$, as indicated by the change of the relative intensities of the bands at 430 and 570 nm (Figure S15, Supporting Information). These fluorescence results are

DOI: 10.1021/acs.joc.5b00275
J. Org. Chem. 2015, 80, 4430−4442

consistent with the changes observed in the absorption spectra when the concentration of $4H^+$ was altered.

Addition of a protic solvent (H_2O) to the CH_3CN solution strongly quenches the fluorescence of **2**–**4**. This finding indicates that a protic solvent opens an efficient deactivation channel from S_1. As discussed above, **2**–**4** populate CT states in a polar solvent wherein the pyridine nitrogen becomes more basic and the pyrrole more acidic. Therefore, quenching of fluorescence in the presence of protic solvent can be rationalized by ESPT leading to the protonation of the pyridine nitrogen and/or deprotonation of the pyrrole NH (Scheme 4). Furthermore, a new shoulder appears (λ > 550 nm) in the fluorescence spectrum of **4** taken in CH_3CN–H_2O (Figure S5, S6, S11, and S12, Supporting Information) that is associated with the fluorescence of $4H^+$ formed by ESPT (see below). Decays of fluorescence of **2**–**4** in CH_3CN–H_2O were multiexponential, but due to the presence of a very fast component, analysis of the decay components was not possible with the SPC equipment used.

Acid–base properties were investigated for **2**–**4** by UV–vis and fluorescence titrations. For *para* derivative **4**, the pH titrations were performed in H_2O in the absence of a buffer and in the presence of phosphate or citrate buffers at two different concentrations of **4**. The variation of pH in the range 3–7 induced UV–vis and fluorescence spectral changes (Figure 2).

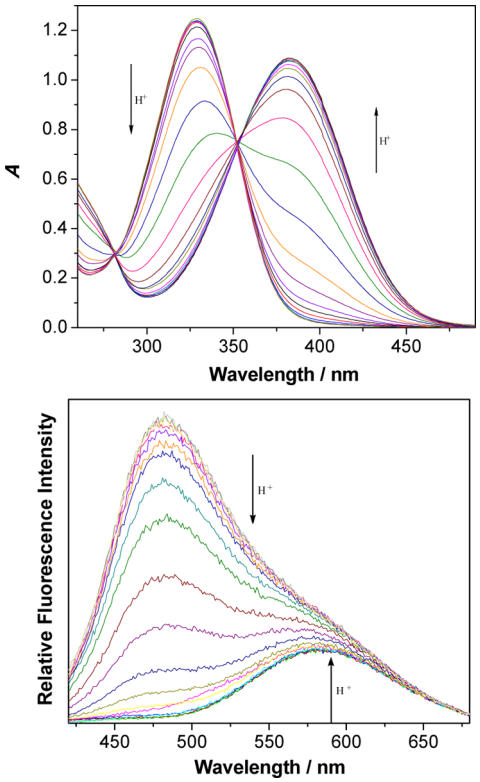

Figure 2. UV–vis (top, [**4**] = 5.3 × 10^{-5} M) and fluorescence spectra (bottom, λ_{ex} = 350 nm, [**4**] = 5.3 × 10^{-6} M) at different pH values (from 3.0 to 7.5) in the presence of citrate buffer (0.05 M).

These spectra were processed by multivariate nonlinear regression analysis using the SPECFIT software[54−56] to reveal the pK_a of 5.5 ± 0.1 determined using different methods (Figure S26–S37 and Table S9, Supporting Information). This value matches the pK_a for the protonation of the pyridine nitrogen (pK_a = 5.2).[57] Similar spectral changes were observed in the UV–vis pH titrations of **2** and **3** (Figures S16, S17, S22, and S23, Supporting Information) which were processed by SPECFIT software to reveal the pK_a values of ∼4.8 (see Tables S7 and S8, Supporting Information).

The pK_a* value for the protonation of the pyridine nitrogen in **4** in S_1 was estimated from the fluorescence titration by use of the Förster cycle.[3] Nonlinear regression analysis of the fluorescence titration data revealed the position of the emission maxima in aqueous solution for **4** and $4H^+$ at 484 and 580 nm, respectively (Table S9, Supporting Information). These values correspond to the increase of basicity of the pyridine nitrogen on excitation to S_1 of ΔpK = 7.2 ± 0.2; that is, the estimated value of pK_a* is 12.7 ± 0.2. For **2** and **3** Förster cycle analysis could not be applied to determine pK_a* for the protonation of pyridine since the corresponding protonated form $2H^+$ is not fluorescent and due to generally very weak fluorescence of both **3** and $3H^+$ (see Figures S18–S21, S24, and S25, Supporting Information). In contrast to pyridine, pyrrole behaves as a weak acid. The reported pK_a value for deprotonation of pyrrole is 17.5.[57] Therefore, we could not determine the pK_a for the deprotonation of pyrrole for compound **4** in the aqueous solution.

Inclusion Complex with Cucurbit[7]uril (CB[7]). Positively charged $4H^+$ is a good candidate to form a host–guest complex with CB[7]. This macrocyclic host is known to bind guests well with positive charges and hydrophobic moieties,[42] where the hydrophobic moiety fits within the cavity of the CB[*n*] and the positive charge is stabilized by interaction with the carbonyl groups. The association equilibrium constant was determined by UV–vis titration. To ensure that the solution contained only $4H^+$, the titration was performed at pH 3.5 in the presence of citrate buffer. Addition of CB[7] induced a hypochromic and very weak bathochromic shift indicative of complex formation (Figure 3). An overall binding model with

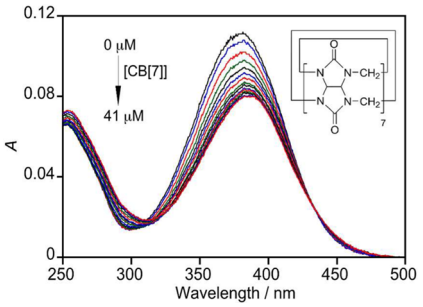

Figure 3. Absorption spectra for $4H^+$ (5 μM) in citrate buffer (47 mM, pH = 3.5, [Na^+] 39 mM) in the absence and presence of different concentrations of CB[7].

the formation of a 1:1 complex between $4H^+$ and CB[7] was employed (see the Supporting Information) where the binding of sodium cations (39 mM) to CB[7] was not accounted for in separate equilibria. The overall binding constant[58] β_{11} of (1.0 ± 0.2) × 10^5 M^{-1} was determined from two independent experiments for the absorption change at 360, 380, and 390 nm (Figure S38–S39 and Table S11, Supporting Information).

Complexation with CB[*n*] changes the pK_a of bound guest molecules,[59,60] and therefore, influences ESIPT reactivity of complexed guests.[61] This variation of pK_a upon complexation was used for logic gates[62] or drug delivery systems.[63−65] Therefore, we investigated the use of CB[*n*] to modulate the pK_a of **4** by performing titrations with CB[7] in nonbuffered

DOI: 10.1021/acs.joc.5b00275
J. Org. Chem. 2015, 80, 4430–4442

solution wherein the formation of the inclusion complex is anticipated to lead to the pyridine protonation. In the titration experiment, an aqueous solution of CB[7] containing 100 mM NaCl was added to solutions of **4** in CH_3CN-H_2O (1:9 or 1:99, both containing 100 mM NaCl). The band at 330 nm disappeared with concomitant formation of a new band at 390 nm (Figure 4 and Figure S40 in the Supporting Information).

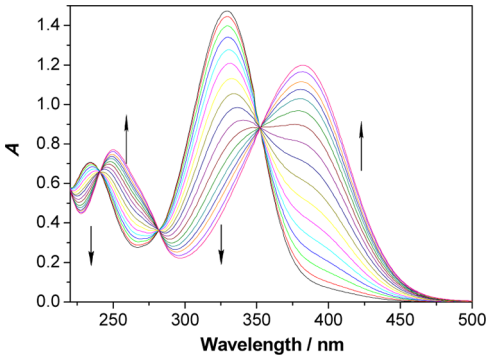

Figure 4. Absorption spectra for the titration of **4** (5×10^{-5} M in CH_3CN-H_2O 1:10, 100 mM NaCl) with CB[7] (1 mM in H_2O, 100 mM NaCl, CB[7] = 0–6×10^{-5} M) in the absence of buffer. The curves were corrected for dilution.

The titration data resemble the ones seen in the pH titration (Figure 2 top), where the absorption with maximum at 390 nm corresponds to $\mathbf{4H^+}$. This finding indicates that CB[7] enhances the basicity of **4**, leading to a stabilization of $\mathbf{4H^+}$ in the inclusion complex.

To determine the pK_a of $\mathbf{4H^+}$ in the CB[7] complex we performed a pH titration of **4** in the presence of a large excess of CB[7] (0.5 mM) to ensure that all **4** is bound to the complex, since it is known that the neutral form of guests have a lower stability constants than the cationic forms.[38,42,43] The resulting UV–vis spectra (Figure S41, Supporting Information) were processed by multivariate nonlinear regression analysis using the SPECFIT program[54–56] to reveal a pK_a value of 6.97 ± 0.05. The higher pK_a value ($\Delta pK_a \approx 1.5$) is in accordance with literature precedent.[59,60]

Laser Flash Photolysis (LFP). LFP measurements for CH_3CN and CH_3CN-H_2O solutions were performed for isomers **2**–**4** as well as for the salt of $\mathbf{4H^+}$ to probe for the formation of phototautomers by ESPT. No phototautomers are expected to be formed in CH_3CN. Transient absorption spectra for isomers **2**–**4** in CH_3CN showed an absorption band with a maximum at 410 nm and a weaker band at 680 nm (Figure 5). Addition of H_2O to the CH_3CN solution significantly changed the appearance of the transient absorption (Figure 5 and Figure S42, Supporting Information). The results in CH_3CN (Figure 5, black lines) will be described first where for **2**, **3**, and **4** the same transients were observed (Figure S43–S49, Supporting Information). These were assigned to radical cations **9**, which absorb at 680 nm, and pyrrolyl N-centered radicals (**10**), which absorb at 410 nm (Scheme 5) according to the comparison with published transient spectra for phenylpyrroles[66] and indoles.[67,68] The decay of the transient absorption measured in CH_3CN was fit to a sum of two exponentials ($k \approx 9 \times 10^5$ s^{-1} and 1×10^5 s^{-1} for **2**, 1×10^6 s^{-1} and 1×10^5 s^{-1} for **3**, and 3×10^5 s^{-1} and 10^4 s^{-1} for **4**). The lifetimes were not affected by O_2, in agreement with a previous report that O_2 does not quench N-centered radicals[69] and

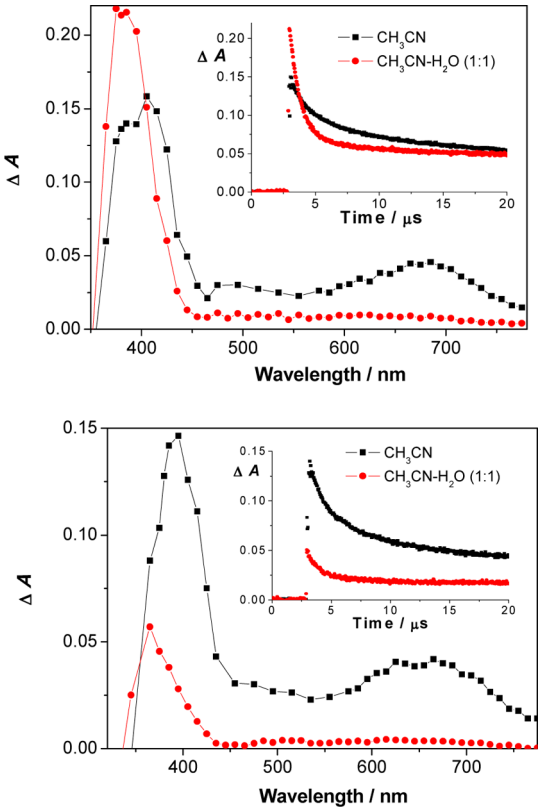

Figure 5. Transient absorption spectra in O_2 purged and optically matched ($A_{355} \approx 0.35$) solutions for **2** (top) in CH_3CN (delay = 500 ns) and in CH_3CN-H_2O (delay = 200 ns); the inset shows the decays at 380 nm). Transient absorption spectra in O_2 purged and optically matched ($A_{355} \approx 0.32$) solutions for **3** (bottom) in CH_3CN (delay = 600 ns) and CH_3CN-H_2O (delay = 200 ns); the inset shows the decays at 380 nm.

Scheme 5. Photochemistry of 2–4 in Aprotic Solvent

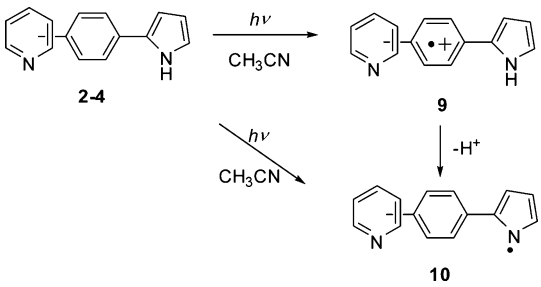

radical cations.[66–69] Short-lived **9** absorbing in the visible part of the spectrum and long-lived **10** absorbing at shorter wavelengths (380–420 nm) are probably formed in parallel processes. However, the observation of a growth kinetics with small amplitude in the transient absorption at 420 nm (Figure S48, SI) suggested that sequential formation of **9** and decay of this transient leading to the longer lived **10** may also take place. Since the absorption of solvated electron was not detected, an electron acceptor in the formation of **9** could have been an $H^\bullet$ radical, which is produced in the parallel process, traces of O_2 or H_2O molecules, or **2**–**4** in S_0 (less likely since radical anions of **2**–**4** were not detected). Furthermore, in the homolytic cleavage of the pyrrole N–H bond and formation of **10**, H-acceptors could have been **2**–**4** in S_0, CH_3CN, or O_2 molecules.

DOI: 10.1021/acs.joc.5b00275
J. Org. Chem. 2015, 80, 4430–4442

In CH_3CN-H_2O solution of **2**–**4**, the transient absorption band in the visible region was not detected (Figure 5 and Figures S43–S47 and S49, Supporting Information), in accordance with the assignment of the transient observed in CH_3CN to radical cations, which in aqueous solution rapidly decay by proton transfer giving pyrrolyl radicals. Therefore, transients **9** are not observed when water is present but the absorption of transient **10** is present (vide infra for discussion on lifetimes). In the case of derivatives **2** and **4**, but not **3**, a new transient with absorption between 380 and 420 nm (Figure 5 and Figures S42–S47 and S49, Supporting Information) was observed that is assigned to phototautomers **2-T** (vide infra, Scheme 7) and **4-T** (Scheme 4) formed by ESPT. These species gave rise to a higher intensity of the transient absorbance at 380–420 nm, compared to the spectra in CH_3CN solutions when the absorbance values at the excitation wavelengths were matched (Figure 5 top). In the case of **3**, analysis of the kinetics (vide infra) showed that **3-T** was not observed on the nanosecond time scale (Figures S42, S45, and S46, Supporting Information). Therefore, the spectrum in CH_3CN-H_2O (Figure 5 bottom) corresponds only to intermediate **10**.

The relative contribution of the species in the photochemistry of **2**–**4** (Scheme 4) is expected to be pH dependent for reactions in CH_3CN-H_2O because the formation of phototautomers is pH dependent. At pH 11 (Figure 6), the decay of the transient absorption was fit to a single-exponential function (4.1×10^6 s^{-1}, τ = 240 ns) and was assigned to phototautomer **4-T** that at this pH decays through a unimolecular process. A small offset was observed at longer times which suggests that a long-lived transient was present. This transient was more prominent at lower pHs and corresponds to **10** (vide infra).

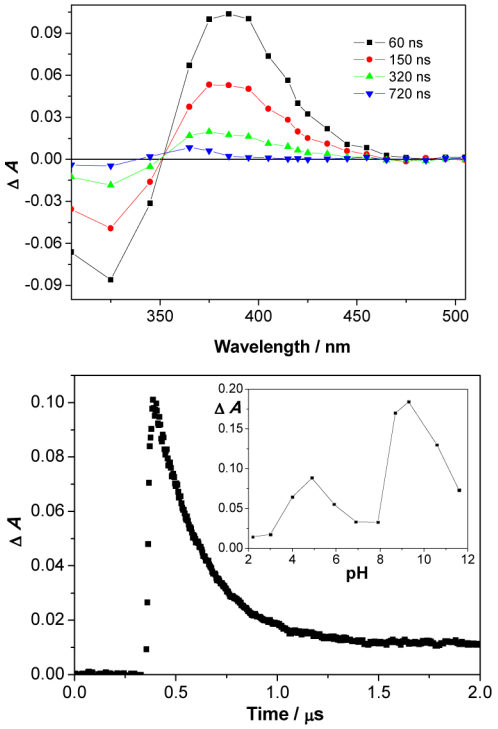

Figure 6. Transient absorption spectra of **4** (top) in CH_3CN-H_2O (5:95), and decay at 380 nm at pH = 11. The inset shows the pH dependence of the transient absorbance intensity at 390 nm, right after laser excitation).

A decrease of the pH from 11 to 9–10 led to slower kinetics, and the decay could not be fit to a monoexponential function. As will be shown below, the kinetics correspond to a combination of bimolecular and unimolecular processes, where the bimolecular process is assigned to the reaction between two molecules of **4-T** which competes with the unimolecular decay of **4-T**. The bimolecular component only becomes apparent when the unimolecular decay of **4-T** becomes slower at these lower pH values. The contribution of the bimolecular process was minimized by decreasing the energy of the laser pulse and the decay was fit by starting the fits at successively longer delay times after the laser pulse until the kinetics fit to a monoexponential function (eqs S3 and S4 and Figure S50, Supporting Information). The lifetime for the unimolecular decays of **4-T** were ~2 μs at pH 10 and 4 μs at pH 9. A lengthening of the lifetime of **4-T** is expected since **4-T** undergoes base catalysis to recover **4**. In addition to the decay of **4-T**, another transient was observed that decayed over a much longer time window. This longer decay was fit to a monoexponential function and had a lifetime of 120 μs (k = 8.3×10^3 s^{-1}). This transient is assigned to **10** based on precedent in the literature.[66−69]

On decrease of the pH below 8–9, the characteristic strong signal assigned to **4-T** disappeared. Thus, in neutral and acidic solution only the longer-lived transient species was detected assigned to radical **10**, decaying through a unimolecular process ($k = 8.3 \times 10^3$ s^{-1}, τ = 120 μs). However, between pH values of 3 and 8 a new transient is observed (Figure S51, Supporting Information). The lifetime for this transient was estimated to be shorter than 100 ns, where this decay occurs over a short time window and levels off before the long-lived decay occurs. Since the short-lived transient was not detected in the visible part of the spectrum (at 680 nm), it cannot correspond to radical cation **9′**. According to the observation of the transient only at pH 3–8, its short lifetime, and the absorption at 390 nm, it may be related to the equilibrium between **4** and $\mathbf{4H^+}$ in the ground state (Scheme 4). Upon excitation, singlet excited state **4** is protonated leading to $\mathbf{4H^+}$ because of the higher basicity in S_1. Therefore, this transient was tentatively assigned to an excess of $\mathbf{4H^+}$ in S_0 which then decays to re-establish the ground-state equilibrium between **4** and $\mathbf{4H^+}$.

Formation of **4-T** by ESPT can only be facilitated in the pH range between the pK_a* values for the pyridine protonation and the pyrrole deprotonation. These pK_a* values were estimated in LFP experiments from the dependence of the initial transient absorption intensity right after the laser pulse collected at different pH values (Figure 6, bottom, inset). Although this value is related to the formation of all transients, significantly stronger signal intensities were observed in the pH region between 9 and 12 where the characteristic transient assigned to **4-T** was detected. Thus, the estimated pK_a* from the LFP experiment for the pyrrole deprotonation in S_1 is in the range of 8–9 and for the protonation of the pyridine this range is between 11 and 12 (Scheme 4). The value for the pyridine pK_a* in S_1 for $\mathbf{4H^+}$ obtained by LFP (11–12) is somewhat lower than the value obtained by Förster cycle analysis (12.7). However, it should be noted that the determination of pK_a* by the Förster cycle is usually inacurrate.[3] Irrespective of the accuracy for the pK_a* values, LFP measurements clearly showed that the formation and decay kinetics of phototautomer **4-T** in aqueous solution is pH dependent.

DOI: 10.1021/acs.joc.5b00275
J. Org. Chem. 2015, 80, 4430–4442

In some ESPT systems, double-proton transfer takes place through a bimolecular reaction involving two phototautomers, leading to nonexponential decays for the phototautomers.[9] Therefore, the origin of the nonexponential decays for **2-T** and **4-T** was investigated using LFP by changing the energy of the laser pulses. For competitive uni- and bimolecular reactions, the decrease of the laser pulse energy leads to a decreased contribution of the bimolecular reaction to the observed kinetics, because the bimolecular reaction depends on the concentration of phototautomer, whereas unimolecular reactions are independent of the concentrations of reactants. The contribution of the bimolecular reaction appears as an initial nonlinear decay in the semilog plot of the knetics (Figure 7).

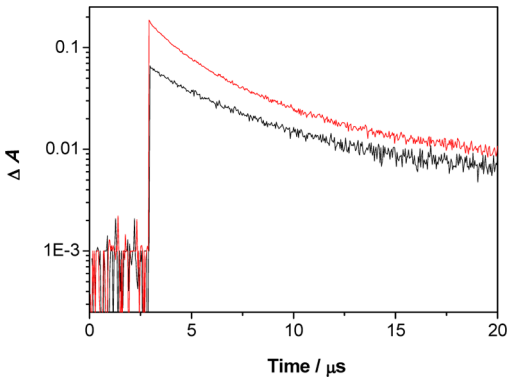

Figure 7. Decay of the log of the transient absorbance at 400 nm for the solution of **4** in CH_3CN-H_2O as a function of the relative laser pulse energy, estimated from the intensity of the benzophenone triplet at 525 nm (black line $\Delta A_{525} = 0.08$; red line $\Delta A_{525} = 0.31$) for optically matched solutions at the excitation wavelength ($A_{355} = 0.31$).

4-fold decrease of the laser pulse energy decreased the amplitude of the bimolecular contribution of the decay. This finding indicates that only one species is detected as decaying by competing uni- and bimolecular reactions. Similar findings have already been reported in the photochemistry of pyridylphenols.[70]

Proton-transfer processes are usually characterized by a large primary isotope effect.[71] To verify the assignment of the transient absorption to **2-T** and **4-T** we conducted LFP measurements for **2** and **4** in optically matched CH_3CN-H_2O and CH_3CN-D_2O solutions (Figure 8 and Figure S52 in the Supporting Information). Changing H_2O to D_2O resulted in weaker signal intensities and longer decay times for both compounds. From the ratio of the transient absorbance intensity immediately after the laser pulse, the estimate for the isotope effect for the formation of tautomers is in the range 1.3−2.5. However, the precise values of the isotope effects for the decay of transients were not warranted due to complex decay kinetics imposed by competing uni- and bimolecular reactions. The observed changes in the decay kinetics and the intensity of the transient absorption are due to the primary deuterium isotope effect for the formation and the decay of the transient species. These results strongly indicate that the observed transient absorption corresponds to species formed by ESPT.

LFP measurements were also conducted for the salt $\mathbf{4H}^+$ in CH_3CN and CH_3CN-H_2O (Figures S53−S56 and S57 left, Supporting Information). In CH_3CN, relatively weak transient absorption was observed with a maximum at 650 nm. The decay was fit to a sum of two exponentials with rate constants

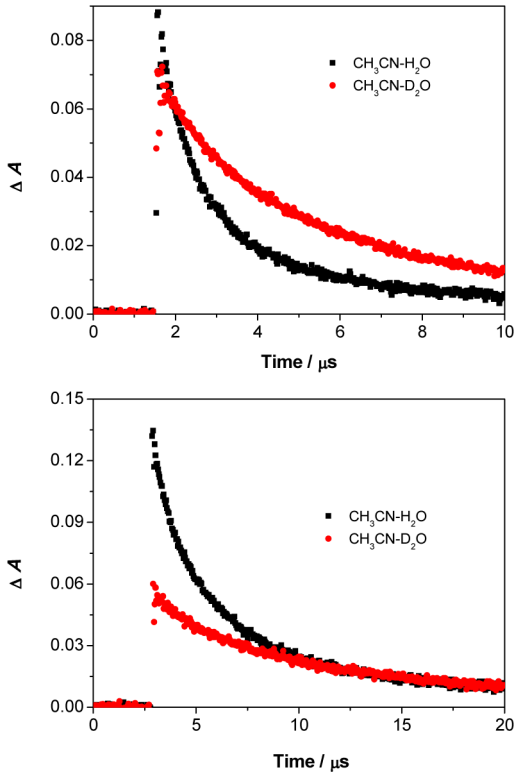

Figure 8. Decay of transient absorbance at 420 nm in CH_3CN-H_2O (1:1) and CH_3CN-D_2O (1:1) for **2** (top) and **4** (bottom).

of 5×10^6 and 2×10^4 s^{-1}. Due to the similarity of the transient absorption with radical cation **9**, the fast component was tentatively assigned to tautomeric radical cation **9′** formed by homolytic N−H cleavage of $\mathbf{4H}^+$, whereas the slow component was assigned to radical **10** (Scheme 6). The measurement in

Scheme 6. Homolytic Cleavage of $4H^+$ Observed in Aprotic Solvent

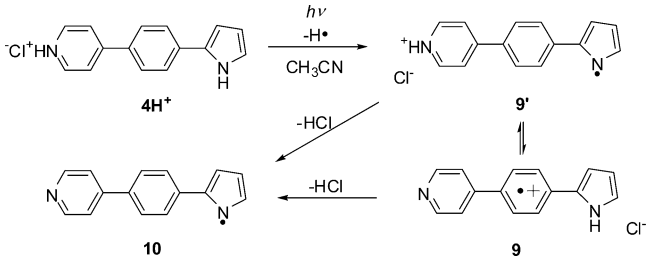

CH_3CN-H_2O performed at neutral or slightly basic conditions gave rise to the same transients as observed by LFP of **4** since $\mathbf{4H}^+$ at pH > 5.5 dissociates. Measurements in the acidic solutions (H_2SO_4, pH 2) gave rise to a transient absorption with a maximum at 370 nm and weaker signals at 390 and 420−500 nm decaying with a rate constant of 4×10^4 s^{-1} that in analogy was assigned to radical **10** (Figure S56, Supporting Information).

LFP experiments were conducted with the $\mathbf{4H}^+$·CB[7] complex to probe if the phototautomerization can take place within the cavity of CB[7]. Interestingly, the complexation with CB[7] completely changed the photochemistry of $\mathbf{4H}^+$. The signals corresponding to the phototautomer **4-T** were not detected. Instead, the transient absorption showed a maximum

DOI: 10.1021/acs.joc.5b00275
J. Org. Chem. 2015, 80, 4430−4442

at 370 nm and a weaker broad band at 500−700 nm, similar to the transients observed in neat CH_3CN after decay of the radical cation (Figure 9 and Figure S58, Supporting Information).

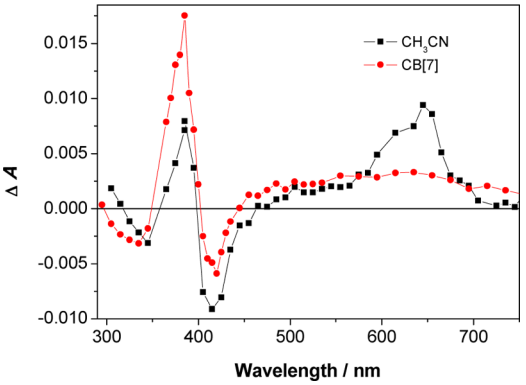

Figure 9. Transient absorption spectra of **4H**$^+$ (4.8×10^{-5} M) in CH_3CN and in aqueous NaCl in the presence of CB[7] (2×10^{-4} M) taken 700 ns after the laser pulse. The solutions were optically matched (A_{355} = 0.35).

Therefore, we assigned the observed transient absorption in the presence of CB[7] to the pyrrolyl radical **10**.

DISCUSSION

Irradiation of **2**−**4** does not yield any stable photoproduct. However, quenching of fluorescence in aqueous solutions and LFP measurements indicate that ESPT takes place in H_2O leading to the formation of phototautomers. Since the acidic site (pyrrole) and the basic site (pyridine) are not in proximity, a polar protic solvent is essential to stabilize the CT character of the S_1 state and, even more important, to act as a proton donor (acid) and acceptor (base).

Formation of phototautomer **2-T** from the *ortho* derivative in aqueous solution was assigned to the transient absorption with a maximum at 390 nm. In near-neutral solution, the decay for **2-T** was not exponential due to competing uni- and bimolecular reactions, as indicated by the dependence of the kinetics on the laser pulse energy. Only an estimate was possible for the decay time of **2-T**, $\tau \approx 1.5$ μs. The assignment of the transient to **2-T** was corroborated by a primary isotope effect in D_2O solutions for its formation and decay (Figure 8). Moreover, **2-T** can in principle exist in two isomeric forms (**2-Ta** and **2-Tb**, Scheme 7). The observed nonexponential decay of **2-T** could in principle originate from the presence of these two isomers that undergo photochemical *E*−*Z* isomerization, and are characterized by different decay rate constants. However, the photochemical *E*−*Z*-isomerization would require a second photon. Furthermore, we observe similar nonexponential decay kinetics for **4-T** which cannot have two stereoisomers. Since the fast decay depends largely on the laser pulse energy, this kinetics is more likely due to the bimolecular reaction of **2-T** involving two proton transfers.

Meta derivative **3** also bears the basic pyridine nitrogen and the acidic pyrrole NH. Strong quenching of fluorescence in aqueous solution strongly indicates deactivation from S_1 by ESPT. Contrary to the transient spectra of **2**, the LFP for the *meta* isomer **3** did not give rise to a characteristic transient absorption that could be assigned to the phototautomer (Figure S42, Supporting Information). Instead, in aqueous solution the transient absorption spectrum was narrower (370−390 nm), and the kinetics was slower than for **2-T**; that is, the fast decay was missing. The transient spectrum of **3** was assigned to pyrrolyl radical **10** (Figure 5 bottom). We do not have data for the acidity/basicity of **3** in S_1 or spectroscopic evidence for the formation of the corresponding phototautomer **3-T**. Nevertheless, **3-T** is a zwitterion that cannot be represented by a Kekulé structure. Therefore, if this transient was formed in aqueous solution it would probably be very short-lived (probably in the picosecond time scale) and could not be detected by nanosecond LFP. However, structurally related more stable zwitterions formed in photodehydration of phenols have been reported and characterized by LFP.[72] The other plausible explanation for the observed quenching of fluorescence of **3** in aqueous solution does not involve ESPT and formation of phototautomer **3-T**. Quenching may occur due to H-bonding with the solvent, leading to a deexcitation via an internal conversion channel.[34−36]

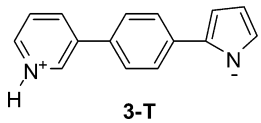

3-T

Excitation of **4** to S_1 leads to a significant enhancement of the pyridine basicity (pK_a^* ≈ 12), as indicated by fluorescence measurements. In addition, concomitant enhancement of the pyrrole acidity in aqueous solution leads to ESPT and formation of phototautomer **4-T**, provided that the solution pH is in the range between the pK_a^* of pyrrole (pH ≈ 8−9) and the pK_a^* of pyridine (pH ≈ 11−12). A water molecule protonates the pyridine nitrogen, and the pyrrole is deprotonated to another water molecule from the solvent leading to the formation of phototautomer **4-T**. Therefore, in the appropriate pH range phototautomer **4-T** was detected by LFP by its characteristic strong transient absorption with a maximum at 390 nm. Phototautomer **4-T** in near-neutral solution (pH 8−10) decays through uni- and bimolecular reactions, as indicated by the dependence of decay on the laser

Scheme 7. Phototautomerization of 2

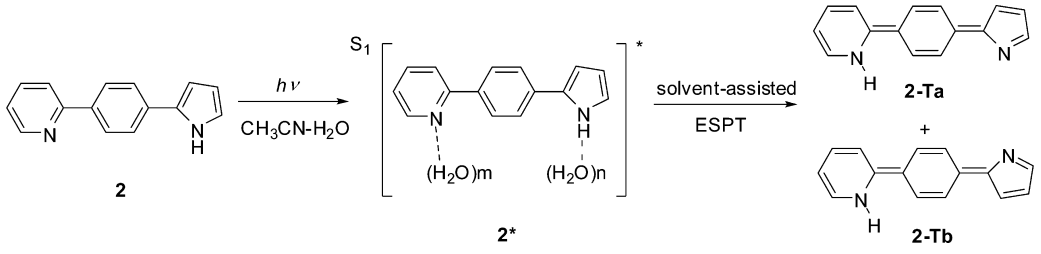

DOI: 10.1021/acs.joc.5b00275
J. Org. Chem. 2015, 80, 4430−4442

pulse energy. As anticipated, the formation and decay of **4-T** are pH dependent and susceptible to deuterium isotope effect. The decay kinetics for **4-T** are probably governed by general and specific acid and base catalysis. Such acid/base catalysis was demonstrated, for example, in the hydration reactions of quinone methides[73] or keto−enol tautomerizations.[74,75]

The driving force for the formation of phototautomer **4-T** was investigated by molecular modeling. The energy for the vertical excitation of **4** to S_1 calculated at the B3LYP/6-311G level of theory in the gas phase is 366 kJmol^{-1} (Scheme 8 and Table S1, Supporting Information), which perfectly matches the experimentally observed absorption of **4** in CH_3CN (λ_{max} = 327 nm, 365.8 kJ mol^{-1}). The S_1 state of **4** has a significant CT character, as evidenced by the fluoro-solvatochromic properties and the calculated dipole moment (Table S3, Supporting Information). The CT character is the driving force for ESPT to occur. The calculated energy of the S_1 state of **4-T** in the gas phase is higher, 390 kJmol^{-1} (Figure S3 and S4 and Tables S2, and S5, Supporting Information). However, we have no evidence that **4-T** is formed in the excited state. Its formation may involve double ESPT by solvent molecules in an adiabatic exergonic reaction, or passing through a conical intersection, leading to **4-T** in S_0.

Scheme 8. Energy Diagram for 4 and 4-T

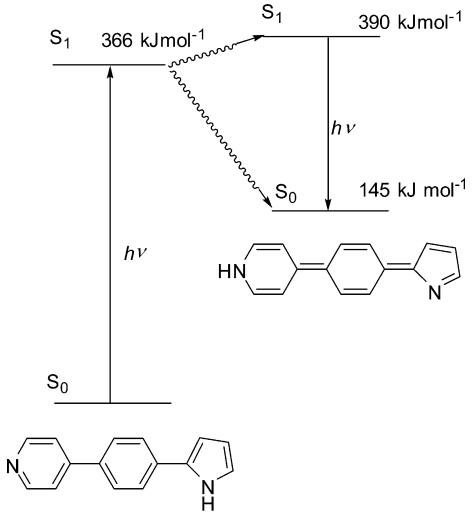

Kinetics for **4-T** formation could not be studied since the tautomerization takes place within the laser pulse (10 ns). Protonation and deprotonation may take place simultaneously or sequentially. Furthermore, we have no experimental evidence if the tautomerization involves a H_2O-relay mechanism as was suggested for 7-azaindoles[18] and 7-hydroxyquinoline.[19−23] Phototautomer **4-T** is 145 kJmol^{-1} higher in energy than **4**, which sets the stage for the tautomerization in the ground state back to the starting molecule, taking place between 200 ns to 4 μs, depending on the pH of the solution.

In an aprotic solvent, excitation of **4** to S_1 leads to parallel reactions, where homolytic cleavage of the pyrrole N−H forms radical **10** and photoionization of **4** forms radical cation **9**. The radical cation is acidic and deprotonates to pyrrolyl radical **10**. Similarly, excitation of **4H**$^+$ in an aprotic solvent ultimately leads to the formation of **10**, involving homolytic cleavage of the pyrrole N−H bond to form radical cation **9**′ followed by deprotonation to **10**. These processes probably also take place in aqueous solution but with a quantum efficiency significantly lower than for the phototautomerization. Therefore, radical **10** can be detected by LFP after the decay of **4-T**. However, the minor pathways involving homolytic cleavage leading to radicals **10** become dominant in acidic aqueous solutions at pH < pK_a* for the deprotonation of pyrrole in S_1.

Positively charged **4H**$^+$ formed a stable host−guest complex with CB[7] with a β_{11} value of (1.0 ± 0.2) × 10^5 M^{-1}. Stabilization of the positive charge in the complex increased the pK_a value of the pyridine nitrogen and presumably decreased the pyrrole acidity. Therefore, within the cavity of CB[7] the pyrrole NH in **4H**$^+$ cannot deprotonate to give phototautomer **4-T**. Instead, the competitive homolytic N−H bond cleavage ultimately leading to the formation of pyrrolyl radical **10** becomes the dominant photochemical process (as presented in Scheme 6). Consequently, the complexation with CB[7] fundamentally changes the reactivity of the molecule so that instead of proton transfer it undergoes homolytic cleavage.

The results presented herein have demonstrated the operation of H_2O-mediated long-range ESPT in terphenyl derivatives **2**−**4**. The ability to control this process by pH and complexation with CB[7] is of particular importance. It implicates the use of the investigated systems for the rational design of functional molecules with potential applications in different research fields such as photochemical switching, drug delivery vehicles, logic gates, sensing, and operation of proton pumps in biological systems, where the photochemistry of these terphenyl derivatives can be modulated by changes in pH or complexation to supramolecular hosts.

■ CONCLUSION

Pyrrolylphenylpyridine terphenyl derivatives **2**−**4** were synthesized and their photophysical properties and photochemical reactivity in phototautomerization reactions was investigated. On excitation to S_1 in polar protic solvents, **2**−**4** populate CT states leading to the enhanced basicity of pyridine and enhanced acidity of pyrrole. The difference in acid−base properties enables excited-state proton transfer (ESPT) giving rise to phototautomers **2-T**, **3-T**, and **4-T**. Phototautomers **2-T** and **4-T** were detected by LFP by their characteristic strong transient absorption at 380−450 nm, whereas zwitterionic **3-T** formed from the *meta* derivative could not be detected probably due to its short lifetime. The decays for **2-T** and **4-T** were nonexponential due to competing mono- and bimolecular reactions. The estimated lifetimes for **2-T** and **4-T** are 1.5 and 4 μs at pH 9, and a shortening of the lifetime of **4-T** was observed at higher pH values. The pyridinium salt **4H**$^+$ forms a stable complex with CB[7] with 1:1 stoichiometry (β_{11} of (1.0 ± 0.2) × 10^5 M^{-1}). The complexation increases the pK_a of **4** and changes its photochemical reactivity. Due to decreased acidity of the pyrrole, phototautomerization in the inclusion complex and the formation of the tautomer does not take place but homolytic cleavage of the pyrrole NH leads to the formation of radicals, as is also observed in nonprotic polar solvents.

■ EXPERIMENTAL SECTION

General Methods. ^{1}H and ^{13}C NMR spectra were recorded at 300 or 600 MHz at rt using TMS as a reference, and chemical shifts were reported in ppm. Melting points were determined using a Mikroheiztisch apparatus and were not corrected. IR spectra were recorded on a spectrophotometer in KBr, and the characteristic peak values were given in cm^{-1}. HRMS were obtained on a MALDI TOF/TOF instrument. Irradiation experiments were performed in a reactor

DOI: 10.1021/acs.joc.5b00275
J. Org. Chem. 2015, 80, 4430−4442

equipped with 16 lamps with the output at 350 nm or a reactor equipped with 8 lamps. During the irradiations, the irradiated solutions were continuously purged with Ar and cooled by a tap water finger-condenser. Solvents for irradiations were of HPLC purity. Chemicals were purchased from the usual commercial sources and were used as received. Solvents for chromatographic separations were used as they are delivered from supplier (p.a. grade) or purified by distillation (CH_2Cl_2). Calculations were performed using Gaussian 03 software.[76]

*2-(4-Bromophenyl)pyridine (**6**).*[44,45] In a refluxing solution of 2-bromopyridine (960 mg, 6.0 mmol) and tetrakis(triphenylphosphine)-palladium(0) (80 mg, 0.07 mmol) in dioxane (20 mL), a solution of *p*-bromophenylboronic acid (**5**, 660 mg, 3.3 mmol) in aqueous K_2CO_3 (20 mL, 2 M) was added dropwise during 8 h under nitrogen. After an additional 8 h of reflux, the reaction was quenched with H_2O (50 mL) and extracted with CH_2Cl_2 (3 × 30 mL). The extracts were dried over anhydrous $MgSO_4$ and filtered, and the solvent was removed on a rotational evaporator. The crude compound was purified using silica column chromatography with CH_2Cl_2/EtOAc (1:1), which afforded pure compound (405 mg, 29%): colorless oil; ^{1}H NMR ($CDCl_3$, 300 MHz) δ/ppm 8.68 (ddd, 1H, J = 1.0, 1.6, 4.8 Hz), 7.87 (d, 2H, J = 8.6 Hz), 7.75 (ddd, 1H, J = 1.6, 8.0, 7.0 Hz), 7.69 (ddd, 1H, J = 1.0, 1.6, 8.0 Hz), 7.59 (d, 2H, J = 8.6 Hz), 7.24 (ddd, 1H, J = 1.6, 4.8, 6.2 Hz).

*3-(4-Bromophenyl)pyridine (**7**).*[49,50] A solution of 3-pyridineboronic acid (200 mg, 1.62 mmol), *p*-dibromobenzene (766 mg, 1.63 mmol), and tetrakis(triphenylphosphine)palladium(0) (40 mg, 0.035 mmol) in dioxane (20 mL) and aqueous K_2CO_3 (20 mL, 2 M) was refluxed for 16 h under nitrogen. The reaction mixture was quenched with H_2O (50 mL) and extracted with CH_2Cl_2 (3 × 30 mL). The organic layer was dried over magnesium sulfate, filtered, and evaporated. The extracts were dried over anhydrous $MgSO_4$ and filtered, and the solvent was removed on a rotational evaporator. The crude compound was purified using silica column chromatography with CH_2Cl_2/EtOAc (1:1), which afforded the pure compound (290 mg, 76%): colorless oil; ^{1}H NMR ($CDCl_3$, 300 MHz) δ/ppm 8.81 (d, 1H, J = 2.2 Hz), 8.61 (dd, 1H, J = 1.6, 4.8 Hz), 7.83 (ddd, 1H, J = 2.2, 4.0, 8.0 Hz), 7.61 (d, 2H, J = 8.4 Hz), 7.44 (d, 2H, J = 8.4 Hz), 7.36 (dd, 1H, J = 4.9, 8.0 Hz).

*4-(4-Bromophenyl)pyridine (**8**).*[48] A solution of dry pyridine (0.8 mL, 10 mmol) in dry ether (100 mL) was cooled to 0 °C under nitrogen, and trifluoromethylsulfonic anhydride (1.68 mL, 10 mmol) was added dropwise with vigorous stirring. The resulting mixture was stirred for 30 min and then cooled to −78 °C. In another flask, *p*-dibromobenzene (2.36 g, 10 mmol) was dissolved in dry ether (15 mL) under nitrogen and cooled to −78 °C. A solution of *n*-butyllithium (2.5 M, 5.2 mL) was added dropwise. The resulting organolithium reagent was cannulated to the flask containing pyridine triflate with vigorous stirring during 10 min, and the mixture was allowed to warm to rt. The reaction was quenched with aqueous NaOH (100 mL, w = 5%) and stirred for 10 min. The organic layer was separated, dried over sodium carbonate, and filtered. Evaporation of the solvent afforded crude 4-(4-bromophenyl)-1-[(trifluoromethyl)-sulfonyl]-1,4-dihydropyridine that was purified on a silica column with hexane/CH_2Cl_2 (1:1). The isolated compound was stirred for 12 h in a mixture of dioxane (20 mL) and aqueous NaOH (20 mL, w = 20%). After dilution with H_2O, the compound was extracted with CH_2Cl_2 (3 × 30 mL). The extracts were dried over anhydrous $MgSO_4$ and filtered, and the solvent was removed on a rotational evaporator to afford the pure compound (585 mg, 25%): pale yellow crystals; ^{1}H NMR ($CDCl_3$, 300 MHz) δ/ppm 8.66 (d, 2H, J = 6.3 Hz), 7.61 (d, 2H, J = 8.6 Hz), 7.50 (d, 2H, J = 8.6 Hz), 7.46 (d, 2H, J = 6.3 Hz).

General Procedure for the Suzuki Coupling and the Boc Deprotection. In a refluxing mixture of bromophenylpyridine (1.9 mmol), tetrakis(triphenylphosphine)palladium(0) (0.095 mmol), and cesium carbonate (3.78 mmol) in toluene (40 mL) under argon was added a solution of *N*-Boc-2-pyrrolylboronic acid (1.9 mmol) dropwise during 8 h. After addition, the resulting solution was refluxed for an additional 2 h and then stirred at rt overnight. The reaction was quenched with H_2O (50 mL), the organic layer was separated, and the aqueous layer was extracted with CH_2Cl_2 (3 × 30 mL). The combined organic extracts were dried over anhydrous $MgSO_4$ and filtered, and the solvent was removed on a rotational evaporator. To the resulting crude compound was added a solution of sodium methoxide prepared from sodium (400 mg, 17.3 mmol) and methanol (100 mL), and the mixture was refluxed under nitrogen for 3 h. The solvent was evaporated, H_2O (50 mL) was added, and extraction with CH_2Cl_2 (3 × 30 mL) was carried out. The combined organic extracts were washed with brine, dried over anhydrous $MgSO_4$, and filtered, and the solvent was removed on a rotational evaporator. The crude compound was purified using silica column chromatography with EtOAc/CH_2Cl_2 (1:4) as eluent.

*2-(4-(1H-Pyrrol-2-yl)phenyl)pyridine (**2**).*[48] In a reaction of 2-(4-bromophenyl)pyridine (**6**, 250 mg, 1.1 mmol), tetrakis-(triphenylphosphine)palladium(0) (90 mg, 0.08 mmol), and cesium carbonate (750 mg, 2.3 mmol) was obtained the crude compound *N*-Boc-2-pyrrolboronic acid (240 mg, 1.0 mmol). After being refluxed with sodium methoxide prepared with sodium (380 mg, 16 mmol) and column chromatography the pure compound was obtained (60 mg, 26%): colorless crystals; ^{1}H NMR (C_6D_6, 300 MHz) δ/ppm 8.62 (d, 1H, J = 4.7 Hz), 8.17 (d, 2H, J = 8.5 Hz), 7.41 (br s, 1H), 7.38 (d, 1H, J = 7.9 Hz), 7.29 (d, 2H, J = 8.5 Hz), 7.14 (dd, 1H, J = 1.5, 7.9 Hz), 6.67 (ddd, 1H, J = 1.2, 4.7, 7.9 Hz), 6.64−6.61 (m, 1H), 6.44−6.41 (m, 1H), 6.37−6.32 (m, 1H); ^{13}C NMR (C_6D_6, 75 MHz) δ/ppm 157.2 (s), 150.0 (d), 137.2 (s), 136.3 (d), 133.9 (s), 131.7 (s), 127.7 (d), 124.2 (d), 121.8 (d), 119.7 (d), 119.4 (d), 110.5 (d), 107.2 (d).

*3-(4-(1H-Pyrrol-2-yl)phenyl)pyridine (**3**).* In a reaction of 3-(4-bromophenyl)pyridine (**7**, 280 mg, 1.2 mmol), tetrakis-(triphenylphosphine)palladium(0) (70 mg, 0.06 mmol), cesium carbonate (780 mg, 2.4 mmol), and *N*-Boc-2-pyrrolboronic acid (250 mg, 1.0 mmol) was obtained the crude compound. After being refluxed with sodium methoxide prepared with sodium (380 mg, 16 mmol) and column chromatography the pure compound was obtained (50 mg, 23%): colorless crystals; mp = 174−176 °C; IR (cm^{-1}, KBr) 3402, 3135, 1607, 1480, 1416, 1106, 843, 792, 728; ^{1}H NMR (C_6D_6, 300 MHz) δ/ppm 9.00 (d,1H, J = 2,1 Hz), 8.54 (dd, 1H, J = 1.5, 4.7 Hz), 7.58−7.44 (m, 1H), 7.41 (d, 1H, J = 8.4 Hz), 7.27 (d, 2H, J = 8.2 Hz), 7.19 (d, 2H, J = 8.2 Hz), 6.80 (dd, 1H, J = 4.7, 7.6 Hz), 6.65−6.59 (m, 1H), 6.48−6.43 (m, 1H), 6.39−6.33 (m 1H); ^{13}C NMR (C_6D_6, 150 MHz) δ/ppm 148.8 (d), 148.7 (d), 136.3 (s), 135.6 (d), 133.5 (s), 133.1 (s), 131.5 (s), 124.6 (d), 123.5 (d), 119.5 (d), 110.6 (d), 107.1 (d); HRMS (MALDI-TOF) m/z $[M + e]^-$ calcd for $(C_{15}H_{12}N_2)^-$ 220.0995, found 220.0990.

*4-(4-(1H-Pyrrol-2-yl)phenyl)pyridine (**4**).* In a reaction of 4-(4-bromophenyl)pyridine (**8**, 75 mg, 0.34 mmol), tetrakis-(triphenylphosphine)palladium(0) (40 mg, 0.034 mmol), cesium carbonate (220 mg, 0.68 mmol), and *N*-Boc-2-pyrrolboronic acid (72 mg, 0.30 mmol) was obtained the crude compound. After preparative TLC on silica with ethyl acetate/dichloromethane (1:4) as eluent, the crude was refluxed with sodium methoxide prepared with sodium (380 mg, 16 mmol) and column chromatography to obtain the pure compound (52 mg, 74%): pale yellow crystals; mp = 170−172 °C; IR (cm^{-1}, KBr) 3122, 1593, 1488, 1413, 1283, 1222, 1116, 992, 818, 726; ^{1}H NMR ($CDCl_3$, 300 MHz) δ/ppm 8.65 (d, 2H, J = 6.2 Hz), 8.62−8.53 (m, 1H), 7.66 (d, 2H, J = 8.4 Hz), 7.58 (d, 2H, J = 8.4 Hz), 7.52 (d, 2H, J = 6.2 Hz), 6.94−6.90 (m, 1H), 6.64−6.60 (m, 1H), 6.36−6.31 (m, 1H); ^{13}C NMR ($CDCl_3$, 75 MHz) δ/ppm 150.2 (d), 147.6 (s), 135.3 (s), 133.4 (s), 131.1 (s), 127.4 (d), 124.2 (d), 121.1 (d), 119.4 (d), 110.4 (d), 106.8 (d); HRMS (MALDI-TOF): m/z $[M + H]^+$ calcd for $(C_{15}H_{13}N_2)^+$ 221.1073, found 221.1074.

By adding an etheral solution of HCl to the solution of **4** in dry ether, the hydrochloride salt **4H**$^+$ precipitated quantitatively. The salt was filtered and washed with ether to afford yellow-green crystals: mp = 186−188 °C; IR (cm^{-1}, KBr) 3415, 3250, 1633, 1601, 1481, 1297, 1125, 802; ^{1}H NMR (DMSO-d_6, 300 MHz) δ/ppm 11.56 (s, 1H), 8.85 (d, 2H, J = 6.0 Hz), 8.33 (d, 2H, J = 6.0 Hz), 8.05 (d, 2H, J = 8.2 Hz), 7.85 (d, 2H, J = 8.2 Hz), 7.00−6.94 (m, 1H), 6.79−6.72 (m, 1H), 6.23−6.15 (m, 1H); ^{13}C NMR (DMSO-d_6, 75 MHz) δ/ppm 143.0 (s), 135.9 (s), 130.5 (s), 129.9 (s), 128.4 (d), 123.9 (d), 122.4 (d), 121.1 (d), 109.7 (d), 107.9 (d).

DOI: 10.1021/acs.joc.5b00275
J. Org. Chem. 2015, 80, 4430−4442

Steady-State and Time-Resolved Fluorescence Measurements. Steady-state measurements were performed with a QM-2 fluorimeter (PTI). The samples were dissolved in cyclohexane, CH_3CN, or CH_3CN-H_2O (1:1), and the concentrations were adjusted to absorbances of less than 0.1 at excitation wavelengths of 310, 320, or 330 nm. Solutions were purged with nitrogen for 30 min prior to analysis. Measurements were performed at 20 °C. Fluorescence quantum yields were determined by comparison of the integral of the emission bands with the one of quinine sulfate in 0.05 M aqueous H_2SO_4 (Φ_f = 0.53).[52] For $\mathbf{4H}^+$, acridine yellow in CH_3OH was used as a reference (Φ_f = 0.57).[53] Typically, three absorption traces were recorded (and averaged), and three fluorescence emission traces were collected by exciting the sample at three different wavelengths. Three quantum yields were calculated (eq S1 in the Supporting Information), and the mean value was reported.

Fluorescence decays, collected over 1023 time channels, were obtained on an Edinburgh Instruments OB920 single-photon counter using light-emitting diodes for excitation (excitation wavelength 335 nm or 310 nm for cyclohexane solutions). The instrument response functions (using LUDOX scatterer) were recorded at the same wavelengths as the excitation wavelength and had a half width of ~0.2 ns. Emission decays for samples in CH_3CN solutions were recorded at 410, 430, and 450 nm, while in cyclohexane solutions the decays were measured at 360, 370, and 390 nm. The counts in the peak channel were 3×10^3. For aqueous solutions, the decays were collected at 450 and 470 nm until they reached 1×10^3 counts in the peak channel. The time increment per channel was 0.01753 ns. Obtained histograms were fit as sums of exponentials using global Gaussian-weighted nonlinear least-squares fitting based on Marquardt–Levenberg minimization implemented in the Fast software package from Edinburgh Instruments. The fitting parameters (decay times and pre-exponential factors) were determined by minimizing the global reduced chi-square χ^2 and graphical methods were used to judge the quality of the fit that included plots of the weighted residuals vs channel number.

Determination of pK_a and pK_a * for 2–4. *UV–vis Titration.* A stock solution of $\mathbf{4H}^+$ (1.35 mg) was prepared in CH_3CN (20 mL). The stock solution (20 μL) was diluted to 25 mL with H_2O ($[\mathbf{4H}^+] = 5.3 \times 10^{-6}$ M), and this dilute solution was titrated with a diluted solution of NaOH until pH 9 was reached. The pH of this latter solution was decreased to 3.0 with the addition of a diluted solution of HCl. The pH was measured with a pH meter, and UV–vis spectra were recorded. The measurements were performed at 25 °C. The resulting UV–vis spectra were processed by multivariate nonlinear regression analysis using the SPECFIT program. In the analysis, a surface was fit that is defined by all UV–vis spectra from 242 to 486 nm at different pH values.

Alternatively, a stock solution of $\mathbf{4H}^+$ (1.30 mg or 3.42 mg) in CH_3CN (10 or 25 mL) was prepared and diluted with H_2O to achieve a $\mathbf{4H}^+$ concentration of 1.05×10^{-5} M. A series of solutions was prepared by mixing the diluted $\mathbf{4H}^+$solution in a 1:1 ratio with a solution of phosphate buffer of the appropriate pH (obtained by mixing H_3PO_4, NaH_2PO_4, and Na_2HPO_4). The total concentrations of compound and buffer after dilution were 5.3×10^{-6} and 0.05 M, respectively.

For measurements in the presence of citrate buffer, a stock solution was prepared by dissolving $\mathbf{4H}^+$ (3.25 mg), **3** (2.77 mg), or **2** (2.91 mg) in CH_3CN (25 mL), and the solutions were diluted with H_2O to reach a concentration of 1.06×10^{-4} M. A series of solutions was prepared by mixing the diluted $\mathbf{4H}^+$, **3**, or **2** solution in a 1:1 ratio with citrate buffer of the appropriate pH. The total concentrations of compounds and buffer after dilution were 5.3×10^{-5} M and 0.05 M, respectively.

Fluorescence Titration. The solutions of **2**, **3**, and $\mathbf{4H}^+$ (5.3×10^{-6} M) in the presence of citrate buffer (0.05 M) were prepared as described for the UV–vis studies. The pH was measured by a pH meter, and fluorescence spectra at 25 °C were recorded on a spectrometer with slits set for a bandwidth of 10 or 20 nm for the excitation and emission monochromator. The resulting fluorescence spectra were processed by multivariate nonlinear regression analysis using the SPECFIT program. In the analysis, the surface was fit defined by all fluorescence spectra in the wavelength region from 410 to 680 nm.

Determination of the Equilibrium Constant between $\mathbf{4H}^+$ and CB[7]. A stock solution of $\mathbf{4H}^+$ (545 μM) was prepared in CH_3CN. A solution of citrate buffer (47 mM) was prepared by dissolving citric acid monohydrate (0.7122 g) and trisodium citrate dihydrate (0.3807 g) in H_2O (100 mL). The buffer had a pH of 3.5. A solution of CB[7] (597 μM) in H_2O was prepared, to which no NaCl was added. The citrate buffer was used to prepare the solution of $\mathbf{4H}^+$ and had a Na^+ cation concentration of 39 mM. In the titration experiment, $\mathbf{4H}^+$ was diluted with citrate buffer to reach a final concentration of 5 μM. The variations in the absorbance of $\mathbf{4H}^+$ with additions of CB[7] were measured with a UV–vis spectrophotometer. Absorption spectra for blank solutions containing all chemicals except $\mathbf{4H}^+$ were subtracted from the spectra. Corrected absorbance values were used to determine the overall equilibrium binding constant for the complexation between $\mathbf{4H}^+$ and CB[7]. The fitting of the binding isotherm was performed using the Scientist 3 software (see the Supporting Information). A 1:1 binding model was used to fit the data. During the titration, $\mathbf{4H}^+$ solution was diluted by 5% and this dilution was taken into account during the fitting.

Determination of the pK_a for $\mathbf{4H}^+$ Complexed with CB[7]. A stock solution of $\mathbf{4H}^+$ (1.27 mg) in CH_3CN (10 mL) with a concentration of 4.95×10^{-4} M was prepared. A stock solution of CB[7] (1.0×10^{-3} M) was prepared by dissolving CB[7] (75.41 mg, 79% purity determined by titration)[77] in an aqueous solution of NaCl (50 mL of 0.1 M NaCl). A series of solutions was prepared by adding 40 μL of $\mathbf{4H}^+$ to 1.96 mL of the CB[7] solution and then mixing with 2.0 mL of phosphate buffer of the appropriate pH (obtained by mixing NaH_2PO_4 and Na_2HPO_4). The total concentration of $\mathbf{4H}^+$, CB[7], and the buffer after dilution were 4.95×10^{-6}, 5.02×10^{-4}, and 0.05 M, respectively. The pH was measured by a pH-meter, and the UV–vis spectra were recorded. The spectra were corrected by subtracting the spectrum of the solution containing CB[7] (1.96 mL), CH_3CN (40 μL), and the phosphate buffer at pH 6.11 (2 mL). The measurements were performed at 25 °C. The resulting UV–vis spectra were processed by multivariate nonlinear regression analysis using the SPECFIT program. In the analysis the surface was fit defined by 18 UV–vis spectra in the wavelength region from 242 to 486 nm.

Laser Flash Photolysis (LFP). All LFP studies on a system previously described[78] employed as an excitation source a Quanta-Ray Lab 130–4 pulsed Nd:YAG laser at 355 nm from Spectra Physics (<20 mJ per pulse), with a pulse width of 10 ns. Static cells (7 mm × 7 mm) were used and the solutions were purged with nitrogen or oxygen for 20 min prior to performing the measurements. Absorbances at 355 nm were ~0.3–0.4.

For LFP experiments conducted at different pH values, the pH of the aqueous solution was measured by a pH meter and adjusted with H_2SO_4, NaOH, or citrate buffer (c = 0.05 M), and then this aqueous solution was mixed with the CH_3CN solution of **4**. The pH of the resulting CH_3CN-H_2O (1:1) solution was not measured.

■ ASSOCIATED CONTENT

Supporting Information

Computational results, UV–vis and fluorescence spectra, pH titration data for **2**–**4**, titration data for **4** and $\mathbf{4H}^+$ with CB[7], LFP data and ^1H and ^{13}C NMR spectra of new compounds. This material is available free of charge via the Internet at http://pubs.acs.org.

■ AUTHOR INFORMATION

Corresponding Authors

*E-mail: nbasaric@irb.hr.

*E-mail: cornelia.bohne@gmail.com.

Notes

The authors declare no competing financial interest.

DOI: 10.1021/acs.joc.5b00275
J. Org. Chem. 2015, 80, 4430–4442

■ ACKNOWLEDGMENTS

These materials are based on work financed by the Croatian Foundation for Science (HRZZ), the Natural Sciences and Engineering Research Council (NSERC) of Canada, and the University of Victoria.

■ REFERENCES

(1) *Hydrogen-Transfer Reactions*; Hynes, J. T., Klinman, J. P., Limbach, H.-H., Schowen, R. L., Eds.; Wiley-VCH: Weinheim, 2007.
(2) Kwon, J. I.; Park, S. Y. *Adv. Mater.* **2011**, *23*, 3615−3642.
(3) Ireland, J. F.; Wyatt, P. A. H. *Adv. Phys. Org. Chem.* **1976**, *12*, 131−221.
(4) Arnaut, L. G.; Formosinho, S. J. *J. Photochem. Photobiol. A: Chem.* **1993**, *75*, 1−20.
(5) Klöpffer, W. *Adv. Photochem.* **1977**, *10*, 311−358.
(6) Formosinho, S. J.; Arnaut, L. G. *J. Photochem. Photobiol. A: Chem.* **1993**, *75*, 21−48.
(7) Ormson, S. M.; Brown, R. G. *Prog. React. Kinet.* **1994**, *19*, 45−91.
(8) Le Gourrierec, D.; Ormson, S. M.; Brown, R. G. *Prog. React. Kinet.* **1994**, *19*, 211−275.
(9) Kasha, M. *J. Chem. Soc., Faraday Trans. 2* **1986**, *82*, 2379−2392.
(10) Lill, M. A.; Helms, V. *Proc. Nat. Acad. Sci. U.S.A.* **2002**, *99*, 2778−2781.
(11) Faxén, K.; Gilderson, G.; Ädelroth, P.; Brzezinski, P. *Nature* **2005**, *437*, 286−289.
(12) Schäfer, L. V.; Groenhof, G.; Klingen, A. R.; Ullmann, G. L.; Boggio-Pasqua, M.; Robb, M. A.; Grubmüller, H. *Angew. Chem., Int. Ed.* **2007**, *46*, 530−536.
(13) Sobolewski, A. J.; Domcke, W. *ChemPhysChem* **2006**, *7*, 561−564.
(14) Meyer, T. J.; Huynh, M. H. V.; Thorp, H. H. *Angew. Chem., Int. Ed.* **2007**, *46*, 5284−5304.
(15) Hosler, J. P.; Ferguson-Miller, S.; Mills, D. A. *Annu. Rev. Biochem.* **2006**, *75*, 165−187.
(16) Royant, A.; Edman, K.; Ursby, T.; Pebay-Peyroula, E.; Landau, E. M.; Neutze, R. *Nature* **2000**, *406*, 645−648.
(17) Mathias, G.; Marx, D. *Proc. Nat. Acad. Sci.* **2007**, *104*, 6980−6985.
(18) Kwon, O.-H.; Lee, Y.-S.; Park, H. J.; Kim, Y.; Jang, D.-J. *Angew. Chem., Int. Ed.* **2004**, *43*, 5792−5796.
(19) Kohtani, S.; Tagami, A.; Nakagaki, R. *Chem. Phys. Lett.* **2000**, *316*, 88−93.
(20) Park, H.-J.; Kwon, O.-H.; Ah, C. S.; Jang, D.-J. *J. Chem. Phys. B* **2005**, *109*, 3938−3943.
(21) Kwon, O.-H.; Lee, Y.-S.; Yoo, B. K.; Jang, D.-J. *Angew. Chem., Int. Ed.* **2006**, *45*, 415−419.
(22) Park, S.-Y.; Lee, Y.-S.; Kwon, O.-H.; Jang, D.-J. *Chem. Commun.* **2009**, 926−928.
(23) Park, S.-Y.; Jang, D.-J. *J. Am. Chem. Soc.* **2010**, *132*, 297−302.
(24) Smirnov, A. V.; English, D. S.; Rich, R. L.; Lane, J.; Teyton, L.; Schwabacher, A. W.; Luo, S.; Thornburg, R. W.; Petrich, J. W. *J. Chem. Phys. B* **1997**, *101*, 2758−2769.
(25) Mukherjee, T. K.; Panda, D.; Datta, A. *J. Phys. Chem. B* **2005**, *109*, 18895−18901.
(26) Mukherjee, T. K.; Datta, A. *J. Phys. Chem. B* **2006**, *110*, 2611−2617.
(27) Kyrychenko, A.; Wu, F.; Thummel, R. P.; Waluk, J.; Ladokhin, A. S. *J. Phys. Chem. B* **2010**, *114*, 13574−13578.
(28) Kyrychenko, A.; Herbich, J.; Waluk, J. In *Tautomerism Methods and Theories*; Antonov, L., Ed.; Wiley-VCH: Weinheim, 2014; p 49.
(29) Herbich, J.; Rettig, W.; Waluk, J. *Chem. Phys. Lett.* **1992**, *195*, 556−562.
(30) Herbich, J.; Hung, C.-Y.; Thummel, R. P.; Waluk, J. *J. Am. Chem. Soc.* **1996**, *118*, 3508−3518.
(31) Kijak, M.; Zielińska, A.; Chamchoumis, C.; Herbich, J.; Thummel, R. P.; Waluk, J. *Chem. Phys. Lett.* **2004**, *400*, 279−285.
(32) Petkova, I.; Mudadu, M. S.; Singh, A.; Thummel, R. P.; van Stokkum, I. H. M.; Buma, W. J.; Waluk, J. *J. Phys. Chem. A* **2007**, *111*, 11400−11409.
(33) Nosenko, Y.; Wiosna-Sałyga, G.; Kunitski, M.; Petkova, I.; Singh, A.; Buma, W. J.; Thummel, R. P.; Brutschy, B.; Waluk, J. *Angew. Chem., Int. Ed.* **2008**, *47*, 6037−6040.
(34) Kyrychenko, A.; Herbich, J.; Thummel, R. P.; Waluk, J. *J. Am. Chem. Soc.* **2000**, *122*, 2818−2827.
(35) Wiosna, G.; Petkova, I.; Mudadu, M. S.; Thummel, R. P.; Waluk, J. *Chem. Phys. Lett.* **2004**, *400*, 379−383.
(36) Vetohkina, V.; Kijak, M.; Wiosna-Sałyga, G.; Thummel, R. P.; Herbich, J.; Waluk. *Photochem. Photobiol. Sci.* **2010**, *9*, 923−930.
(37) Assaf, K. I.; Nau, W. M. *Chem. Soc. Rev.* **2015**, *44*, 394−418.
(38) Pavari, G.; Reany, O.; Keinan, O. *Isr. J. Chem.* **2011**, *51*, 646−663.
(39) Macartney, D. H. *Isr. J. Chem.* **2011**, *51*, 600−615.
(40) Walker, S.; Oun, R.; McInnes, F. J.; Wheate, N. J. *Isr. J. Chem.* **2011**, *51*, 616−624.
(41) Day, A. I.; Collins, J. G., In: *Supramolecular Chemistry: From Molecules to Nanomaterials*; Steed, J. W., Gale, P. A., Eds.; John Wiley & Sons: New York, 2012.
(42) Lagona, J.; Mukhopadhyay, P.; Chakrabarti, S.; Isaacs, L. *Angew. Chem., Int. Ed.* **2005**, *44*, 4844−4870.
(43) Masson, E.; Ling, X.; Joseph, R.; Kyeremeh-Mensah, L.; Lu, X. *RSC Adv.* **2012**, *2*, 1213−1247.
(44) Butterworth, E. C.; Heilbron, I. M.; Hey, D. H. *J. Chem. Soc.* **1940**, 355−358.
(45) Hey, D. H.; Stirling, C. J. M.; Gareth, H. W. *J. Chem. Soc.* **1955**, 3963−3969.
(46) Martina, S.; Enkelmann, V.; Wegner, G.; Schlüter, A.-D. *Synthesis* **1991**, 613−615.
(47) Aleškoviċ, M.; Basariċ, N.; Mlinariċ-Majerski, K. *J. Heterocycl. Chem.* **2011**, *48*, 1329−1335.
(48) Lucchesini, F. *Tetrahedron* **1992**, *48*, 9951−9966.
(49) Choi-Sledeski, Y. M.; McGarry, D. G.; Green, D. M.; Mason, H. J.; Becker, M. R.; Davis, R. S.; Ewing, W. R.; Dankulich, W. P.; Manetta, V. E.; Morris, R. L.; Spada, A. P.; Cheney, D. L.; Brown, K. D.; Colussi, D. J.; Chu, V.; Heran, C. L.; Morgan, S. R.; Bentley, R. G.; Leadley, R. J.; Maignan, S.; Guilloteau, J.-P.; Dunwiddie, C. T.; Pauls, H. W. *J. Med. Chem.* **1999**, *42*, 3572−3587.
(50) Wakabayashi, S.; Sugihara, Y.; Takakura, K.; Murata, S.; Tomioka, H.; Ohnishi, S.; Tatsumi, K. *J. Org. Chem.* **1999**, *64*, 6999−7008.
(51) Toscano, R. A.; Hernández-Galindo, M. C.; García-Mellado, R. R. O.; Portilla, F. R.; Amábile-Cuevas, C.; Álvarez-Tolenado, C. *Chem. Pharm. Bull.* **1997**, *45*, 957−961.
(52) Montalti, M.; Credi, A.; Prodi, L.; Gandolfi, M. T. In *Handbook of Photochemistry*; CRC Taylor and Francis: Boca Raton, 2006.
(53) Olmsted, J. *J. Phys. Chem.* **1979**, *83*, 2581−2584.
(54) Grampp, H.; Maeder, M.; Meyer, C. J.; Zuberbühler, A. D. *Talanta* **1985**, *32*, 95−101.
(55) Grampp, H.; Maeder, M.; Meyer, C. J.; Zuberbühler, A. D. *Talanta* **1985**, *32*, 257−264.
(56) Grampp, H.; Maeder, M.; Meyer, C. J.; Zuberbühler, A. D. *Talanta* **1985**, *32*, 1133−1139.
(57) Joule, J. A.; Mills, K. *Heterocyclic Chemistry*; Blackwell Publishing: Oxford, 2000.
(58) Tang, H.; Fuentealba, D.; Ho, K. Y.; Selvapalam, N.; Kim, K.; Bohne, C. *J. Am. Chem. Soc.* **2011**, *133*, 20623−20633.
(59) Mohanty, J.; Bhasikuttan, A. C.; Nau, W. M.; Pal, H. *J. Phys. Chem. B* **2006**, *110*, 5132−5138.
(60) Koner, A. L.; Ghosh, I.; Saleh, N.; Nau, W. M. *Can. J. Chem.* **2011**, *89*, 139−147.
(61) Shaikh, M.; Dutta Choudhury, S.; Mothany, J.; Bhasikuttan, A. C.; Nau, W. M.; Pal, H. *Chem.—Eur. J.* **2009**, *15*, 12362−12370.
(62) Pischel, U.; Uzunova, V. D.; Remón, P.; Nau, W. M. *Chem. Commun.* **2010**, *46*, 2635−2637.
(63) Shaikh, M.; Mohanty, J.; Bhasikuttan, A. C.; Uzunova, V. D.; Nau, W. M.; Pal, H. *Chem. Commun.* **2008**, *44*, 3681−3683.

DOI: 10.1021/acs.joc.5b00275
J. Org. Chem. 2015, 80, 4430−4442

(64) Saleh, N.; Koner, A. L.; Nau, W. M. *Angew. Chem., Int. Ed.* **2008**, *47*, 5398−5401.
(65) Parente Carvalho, C.; Uzunova, V. D.; Da Silva, J. P.; Nau, W. M.; Pischel, U. *Chem. Commun.* **2011**, *47*, 8793−8795.
(66) Basarić, N.; Franco-Cea, A.; Alešković, M.; Mlinarić-Majerski, K.; Wan, P. *Photochem. Photobiol. Sci.* **2010**, *9*, 779−790.
(67) Bent, D. V.; Hayon, E. *J. Am. Chem. Soc.* **1975**, *97*, 2612−2619.
(68) Moorthy, P. N.; Hayon, E. *J. Phys. Chem.* **1974**, *78*, 2615−2620.
(69) Fang, X.; Jin, F.; Jin, H.; von Sonntag, C. *J. Chem. Soc., Perkin Trans. 2* **1998**, 259−263.
(70) Basarić, N.; Wan, P. *Photochem. Photobiol. Sci.* **2006**, *5*, 656−664.
(71) Hansen, P. E. In *Tautomerism Methods and Theories*; Antonov, L., Ed.; Wiley-VCH: Weinheim, 2014; p 143.
(72) Basarić, N.; Cindro, N.; Bobinac, D.; Uzelac, L.; Mlinarić-Majerski, K.; Kralj, M.; Wan, P. *Photochem. Photobiol. Sci.* **2012**, *11*, 381−396.
(73) Chiang, Y.; Kresge, A. J.; Zhu, Y. *J. Am. Chem. Soc.* **2000**, *122*, 9854−9855.
(74) Wirz, J. *Pure Appl. Chem.* **1998**, *70*, 2221−2232.
(75) Pelliccioli, A. P.; Šebej, P.; Wirz, J. *Photochem. Photobiol. Sci.* **2012**, *11*, 967−971.
(76) Gaussian 03, Rev E. 01: Frisch, M. J.; Trucks, G. W.; Schlegel, H. B.; Scuseria, G. E.; Robb, M. A.; Cheeseman, J. R.; Montgomery, J. A., Jr.; Vreven, T.; Kudin, K. N.; Burant, J. C.; Millam, J. M.; Iyengar, S. S.; Tomasi, J.; Barone, V.; Mennucci, B.; Cossi, M.; Scalmani, G.; Rega, N.; Petersson, G. A.; Nakatsuji, H.; Hada, M.; Ehara, M.; Toyota, K.; Fukuda, R.; Hasegawa, J.; Ishida, M.; Nakajima, T.; Honda, Y.; Kitao, O.; Nakai, H.; Klene, M.; Li, X.; Knox, J. E.; Hratchian, H. P.; Cross, J. B.; Adamo, C.; Jaramillo, J.; Gomperts, R.; Stratmann, R. E.; Yazyev, O.; Austin, A. J.; Cammi, R.; Pomelli, C.; Ochterski, J. W.; Ayala, P. Y.; Morokuma, K.; Voth, G. A.; Salvador, P.; Dannenberg, J. J.; Zakrzewski, V. G.; Dapprich, S.; Daniels, A. D.; Strain, M. C.; Farkas, O.; Malick, D. K.; Rabuck, A. D.; Raghavachari, K.; Foresman, J. B.; Ortiz, J. V.; Cui, Q.; Baboul, A. G.; Clifford, S.; Cioslowski, J.; Stefanov, B. B.; Liu, G.; Liashenko, A.; Piskorz, P.; Komaromi, I.; Martin, R. L.; Fox, D. J.; Keith, T.; Al-Laham, M. A.; Peng, C. Y.; Nanayakkara, A.; Challacombe, M.; Gill, P. M. W.; Johnson, B.; Chen, W.; Wong, M. W.; Gonzalez, C.; Pople, J. A. Gaussian, Inc., Pittsburgh, PA, 2003.
(77) Yi, S.; Kaifer, A. E. *J. Org. Chem.* **2011**, *76*, 10275−10278.
(78) Liao, Y.; Bohne, C. *J. Phys. Chem.* **1996**, *100*, 734−743.

DOI: 10.1021/acs.joc.5b00275
J. Org. Chem. 2015, 80, 4430−4442